# Transient Stability Assessment of Power Systems With Uncertain Renewable Generation

Hugo N. Villegas Pico
National Renewable Energy Laboratory
Golden, CO 80401, USA
e-mail: HugoNestor.VillegasPico@nrel.gov

Dionysios C. Aliprantis and Xiaojun Lin
Purdue University
West Lafayette, IN 47907, USA
e-mail: {dionysios, linx}@purdue.edu

***Abstract*—The transient stability of a power system depends heavily on its operational state at the moment of a fault. In systems where the penetration of renewable generation is significant, the dispatch of the conventional fleet of synchronous generators is uncertain at the time of dynamic security analysis. Hence, the assessment of transient stability requires the solution of a system of nonlinear ordinary differential equations with unknown initial conditions and inputs. To this end, we set forth a computational framework that relies on Taylor polynomials, where variables are associated with the level of renewable generation. This paper describes the details of the method and illustrates its application on a nine-bus test system.**

***Index Terms*—Power generation dispatch, power system security, power system stability, power system transients.**

## I. Introduction

Transient stability is a classical problem in power system analysis [1]–[3]. Its objective is to determine whether a set of interconnected generators will remain in synchronism after a large disturbance in the bulk transmission system [3]–[6]. Transient stability analysis is based on synchronous generator electromechanical dynamic models. Invariably, the mechanical rotor dynamics are represented by an equation of motion, but the underlying electrical circuit can take various forms depending on the desired level of fidelity. Electromagnetic phenomena with faster time constants, which do not have a significant impact on rotor angle stability, such as stator and network transients, are typically neglected. Transient instability manifests as a separation of rotor angles within one or more rotor "swings".

The transient response depends heavily on the operational state of a power system at the moment of a fault, as well as on the severity (in terms of network location and impedance) and clearing time of the disturbance. Typically, the operational state of a power system is specified by a security-constrained economic dispatch [7], [8], which in practice assumes known (in advance) steady-state conditions. The incorporation of metrics related to transient stability is possible within this deterministic economic dispatch formulation. Numerical integration methods [9], [10], energy functions [11]–[14], and decision-tree techniques [15], [16] are various approaches to this end.

This material is based upon work supported by the National Science Foundation under Grant No. 1442726.

The transient stability problem has been impacted by the proliferation of renewable energy generation. These resources, which are often non-dispatchable, have been displacing conventional thermal generation at scale. Therefore, the pre-fault operational conditions of the synchronous generators are becoming increasingly uncertain (at the time of analysis), since the balance among power generation, demand, and loss needs to be maintained [17]. Furthermore, wind and solar generation is interfaced using power electronic converters, whose response during grid faults is not precisely known. The increased level of uncertainty in our knowledge of both pre-fault state and post-fault dynamic response, is challenging the conventional (deterministic) transient stability assessment.

Uncertainties in power system dynamics have been studied using trajectory sensitivity analysis, probabilistic collocation, and polynomial chaos methods [18]–[21]. Trajectory sensitivity is limited to relatively small uncertainties because it relies on linearization, thus it may be ill-suited to study large disturbances, particularly when the system is prone to instability. To mitigate this issue, second-order trajectory sensitivity has been proposed in [22]. Polynomial chaos methods may fail at correlating uncertainties with outputs because they rely on sampling the uncertainty space [20]. Recently, Lyapunov-based methods have been introduced for robust transient stability assessment [23], [24]. However, the theory has been only developed for power systems represented with simplified low-order component models.

Approaches based on affine arithmetic and zonotope reachability analysis have been proposed as well [25], [26]. These methods enclose the uncertain evolution of the system states in time by employing convex sets (modeled as images of unit hypercubes by affine transformations [27]) and interval vectors. However, they are sensitive to wrapping (i.e., uncontrolled set expansion due to propagation of recurring over-approximations in nonlinear systems) [28]. The wrapping phenomenon occurs when nonlinear dependencies of states on initial conditions are not considered [29], [30]. When such expansion of sets occurs, one cannot readily differentiate between a physical instability or numerical issues.

An alternative approach to analyze uncertainties relies on Taylor models [28]–[32], which are better suited for propagating the dependency of uncertain initial conditions in nonlinear systems. In addition, Taylor polynomials are relatively simple

to implement in a computer. The main idea of such methods is to calculate multivariate polynomials representing the solution at particular points in time, where the variables are associated with uncertainties of initial conditions. The Taylor model-based approach has been used in transient stability assessment of uncertain power systems in [33]. Therein, the technique was introduced as a tool to study the impact of uncertain inertia constants and initial conditions, which were selected as arbitrary intervals around an equilibrium, thereby lacking rigorous justification. In [33], the power balance constraint among generation and demand is disregarded, hence the initial condition sets are not physically meaningful. Also, the system model of [33] is relatively simple, as it employs reduced-order generator models, and excitation system dynamics are neglected.

This manuscript builds upon the ideas of [28]–[32]. Herein, uncertainties are assumed to originate from the variability of renewable power sources, which in turn impacts the operational conditions of conventional generation. In contrast to [33], we account for the effect of excitation on transient stability by using higher-order models of generators, exciters, and controls. In addition, we calculate sets of initial conditions that satisfy a power balance constraint between uncertain generation and demand before a transient event occurs. This is necessary to have physically feasible sets of initial conditions, thus avoiding unrealistic pre-fault non-equilibrium states. Compared to [25], [26], the wrapping effect is avoided by propagating via multivariate polynomials the nonlinear dependence of the system states on initial conditions.

A concise summary of the proposed method is given in Section II. A model that is suitable for the first-swing transient stability analysis of a multi-machine power system is described in Section III. In particular, the calculation of polynomials that capture uncertain initial conditions and inputs is presented in Section III-E. The method's algorithmic implementation is described in Section IV. Section V presents illustrative results, and Section VI concludes.

## II. Proposed Analysis Framework

The dynamic response of a power system immediately after a transmission fault is calculated by solving an Ordinary Differential Equation (ODE) of the form

$$\frac{d}{dt}z = F_\gamma\left(z, u\right) \tag{1}$$

for $t \in [0, T]$, with initial condition $z_0 \in \mathcal{Z}_0 \subseteq \mathbb{R}^{n_z}$, input $u \in \mathcal{U} \subseteq \mathbb{R}^{n_u}$, and $\gamma \in \{1, 2\}$. The output is defined as a function of the state vector,

$$w = G_\gamma(z)\,. \tag{2}$$

The vector $z$ includes machine electrical and mechanical states, as well as exciter states.[1] The exogenous input vector $u$ contains the prime mover torques at the generator shafts. In order to capture renewable generation uncertainty at the moment of the fault, the initial conditions $z_0$ and inputs $u$ belong to sets $\mathcal{Z}_0$ and $\mathcal{U}$, respectively. In particular, $u$ is considered constant within the time-frame of interest. The ODE is indexed by $\gamma$ to capture the dynamics during the fault ($\gamma = 1$) and after it has been cleared ($\gamma = 2$). The switch occurs at a predetermined clearing time.

A multivariate polynomial vector is defined by

$$y(p) = \sum_{i=1}^{n_\psi} \psi_i(p)\, y_i \tag{3}$$

where

$$\psi_i(p) = \prod_{j=1}^{n_p} p_j^{n_{i,j}} \tag{4}$$

is a monomial on $n_p$ variables $p_1, \ldots, p_{n_p}$, and $y_1, \ldots, y_{n_\psi}$ is a set of $n_\psi$ vectors in $\mathbb{R}^{n_y}$. The polynomial $y(p)$ has a prescribed degree $n_d$. Hence, the exponents $n_{i,j}$ belonging to the $i$-th monomial $\psi_i(p)$ ($i = 1, \ldots, n_\psi$) must satisfy $\sum_{j=1}^{n_p} n_{i,j} \leq n_d$. In this case, the number of possible monomials is $n_\psi = \frac{(n_p+n_d)!}{n_p!n_d!}$ [29], [34]. Herein, all polynomials are of degree $n_d$, and all $n_\psi$ monomials are assumed to be present.

Sets are defined as

$$\mathcal{Y} = \{y(p) : p_j \in [-1, 1],\, j = 1, \ldots, n_p\}\,. \tag{5}$$

Note that each variable $p_j$ represents an independent source of uncertainty. For instance, the sets $\mathcal{Z}_0$ and $\mathcal{U}$ are defined as the range of the vectors of multivariate polynomials $z_0(p)$ and $u(p)$, respectively. Also, the range of various polynomials that are calculated in Algorithm 1 of Section IV represents the sets of power system states and outputs at particular times.

The proposed method relies on algebraic operations between polynomials of order $n_d$, such as addition or multiplication by a constant. When multiplying polynomials, terms of degree greater than $n_d$ are neglected [35]. Disregarding high-order terms does not lead to relatively large error since $|p_j| \leq 1$. In addition, the analysis requires the calculations of function compositions with polynomials, such as trigonometric and exponential functions appearing in the system equations, using $n_d$-order truncated Taylor series [35], e.g., see Appendix A. Based on our experience, polynomial expansions of order as low as $n_d = 3$ can be suitable for the treatment of uncertainties in a transient stability program. All operations and functions can be implemented efficiently in a computer.

The solution to (1) is approximated by computing recursively a sequence of polynomials $z_s(p)$ indexed by $s = 1, 2, \ldots, s_n$ that represent the uncertain states at any time $t = sr$ (the study horizon is $T = s_n r$), where $r$ is a small time step. Each $z_s(p)$ is computed via successive approximations (Picard iterations) [36]–[38]

$$\zeta_s^{(v)}(p, \tau) = z_{s-1}(p) + \int_0^\tau \mathsf{F}_s^{(v-1)}(p, \mu)\, d\mu \tag{6}$$

[1]The prime mover and governor dynamics are not modeled here since we are focusing on first-swing stability, although they could be added for studying multi-swing stability [4].

with

$$\mathsf{F}_s^{(v-1)}(p,\tau) \approx F_\gamma\left(\zeta_s^{(v-1)}(p,\tau), u(p)\right) \tag{7}$$

for $v = 1, \ldots, n_d$. The approximation of (7) occurs because terms of order greater than $n_d$ are dropped. Here, $\tau \in (0, r]$ and $\zeta_s^{(0)}(p,\tau) = z_{s-1}(p)$. Note that $t = (s-1)r + \tau$ during step $s$, hence $z_s(p) = \zeta_s^{(n_d)}(p,r)$.

To begin the recursion, the polynomials $z_0(p)$ and $u(p)$ are calculated from a prescribed vector polynomial that models uncertain dispatch conditions, as detailed in Section III-E. Recall that $u(p)$ is considered time invariant throughout the study, and that it represents the mechanical torques at the shafts of the synchronous machines. In each Picard iteration, a vector polynomial $\mathsf{F}_s^{(v-1)}(p,\tau)$ is calculated from $F_\gamma(\cdot,\cdot)$ by using function compositions with polynomials via Taylor expansions [35], e.g., see Appendix A. Therefore, the function $F_\gamma(\cdot,\cdot)$ is required to be analytic [32]. This is not overly restrictive since the network change due to breaker action can be made to occur close to any given time $t_c = s_c r$ with reasonably small time step. An illustrative example of this iterative procedure can be found in Appendix B.

## III. System Modeling for Transient Stability

### A. Synchronous Generators

The transient response of the $k$-th synchronous generator, $k = 1, \ldots, n$, can be modeled using the following set of ODEs [6]:

$$\frac{d}{dt}e^r_{qd,k} = -T^{-1}_{dqo,k}(e^r_{qd,k} - X_{dq,k}i^r_{qd,k} - e^r_{fd0,k}) \tag{8}$$

$$\frac{d}{dt}\omega_k = \frac{1}{2H_k}\left(T_{m,k} - e^{rT}_{qd,k}i^r_{qd,k}\right) \tag{9}$$

$$\frac{d}{dt}\delta_{k,1} = \omega_b(\omega_k - \omega_1) \quad (k \neq 1)\,. \tag{10}$$

These equations employ per unit quantities. They represent 1.1-type models, i.e., *qd* circuits that have one damper in the *q*-axis and only the field winding in the *d*-axis. (The use of higher-order models is possible.) The superscript '$r$' denotes that the variables are in the rotor reference frame of each machine. Magnetic saturation is not modeled in detail, since the reactances are constant. Stator transients are neglected, as typically done in transient stability studies. The vectors $f^r_{qd,k} = (f^r_{q,k}, f^r_{d,k})^T$ represent either voltage or current; also, we define $e^r_{fd0,k} = (e^r_{fd,k}, 0)^T$ for notational convenience. Machine reactances and time constants are embedded in the matrices

$$X_{dq,k} = \begin{pmatrix} 0 & X'_{d,k} - X_{d,k} \\ X_{q,k} - X'_{q,k} & 0 \end{pmatrix} \tag{11}$$

and $T_{dqo,k} = \mathrm{Diag}(\tau_{do,k}, \tau_{qo,k})$. It is assumed that $X'_{d,k} = X'_{q,k}$, i.e., transient saliency is neglected. The vectors $e^r_{qd,k}$, $i^r_{qd,k}$, $e^r_{fd0,k}$ represent voltages behind transient reactance, currents injected into the power network, and excitation voltage, respectively. The states $\omega_k$ and $\delta_{k,1} = \theta_k - \theta_1$, $k \neq 1$, are rotor speed and relative rotor angle, respectively. The rotor angles $\theta_k$ with $k = 1, \ldots, n$ are measured with respect to a synchronously rotating frame of constant base frequency $\omega_b$, and satisfy $d\theta_k/dt = \omega_b(\omega_k - 1)$. The prime mover torque $T_{m,k}$ are considered a constant input during the study.

### B. Excitation Systems

The exciter, stabilizing circuit, and voltage amplifier for the $k^{\text{th}}$ generator are modeled using the following set of ODEs [6]:[2]

$$\frac{d}{dt}e^r_{fd,k} = -\frac{1}{T_{E,k}}\left[\left(K_{E,k} + S_{E,k}(e^r_{fd,k})\right)e^r_{fd,k} - v_{a,k}\right] \tag{12}$$

$$\frac{d}{dt}r_{f,k} = -\frac{1}{T_{F,k}}\left(r_{f,k} - \frac{K_{F,k}}{T_{F,k}}e^r_{fd,k}\right) \tag{13}$$

$$\frac{d}{dt}v_{a,k} = -\frac{1}{T_{A,k}}\left(v_{a,k} - K_{A,k}v^{\text{in}}_k + S_{A,k}(v_{a,k})\right)\,. \tag{14}$$

For notational simplicity, these states are collected in the vectors $e^{rT}_{fd} = (e^r_{fd,1}, \ldots, e^r_{fd,n})$, $r^T_f = (r_{f,1}, \ldots, r_{f,n})$, and $v^T_a = (v_{a,1}, \ldots, v_{a,n})$. The voltages

$$v^{\text{in}}_k = V^{\text{ref}}_k - V_k + r_{f,k} - \frac{K_{F,k}}{T_{F,k}}e^r_{fd,k} \tag{15}$$

are inputs of (14), where $V^{\text{ref}}_k$ and $V_k$ are reference and measured voltages at the terminals of the $k^{\text{th}}$ generator, respectively. The measured voltage is obtained with[3]

$$V_k = \sqrt{v^{rT}_{qd,k} \cdot v^r_{qd,k}} \tag{16}$$

$$v^r_{qd,k} = e^r_{qd,k} + \begin{pmatrix} 0 & -X'_{d,k} \\ X'_{q,k} & 0 \end{pmatrix} i^r_{qd,k}\,. \tag{17}$$

Note that in this model, the initial condition (at steady state) of the amplifier state satisfies $v_{a,k0} = 0$. The parameter $K_{E,k}$ of (12) depends on $e^r_{fd,k0}$ ($e^r_{fd,k}$ at $t = 0$), i.e., $K_{E,k} = -S_{E,k}(e^r_{fd,k0})$ [40]. The saturation functions for the exciter and amplifier states are, respectively:

$$S_{E,k}(e^r_{fd,k}) = A_{E,k}e^{B_{E,k}e^r_{fd,k}} \tag{18}$$

$$S_{A,k}(v_{a,k}) = \left(K_{A,k} - V^{\text{lim}}_{A,k}\right)\left(\frac{v_{a,k}}{V^{\text{lim}}_{A,k}}\right)^\sigma\,. \tag{19}$$

The exponent $\sigma$ can take odd values, i.e., $\sigma \in \{3, 5, 7, \ldots\}$. The function $S_{A,k}(v_{a,k})$ is introduced to saturate the amplifier state smoothly instead of using hard limits, so that $-V^{\text{lim}}_{A,k} \leq v_{a,k} \leq V^{\text{lim}}_{A,k}$. If the value of the exponent $\sigma$ is relatively high, the behavior of the amplifier with smooth saturation approaches the model using hard limits. However, this requires increasing the order of Taylor polynomials, which could become computationally impractical. The response of the excitation system obtained by the smooth saturation model is shown in Fig. 1 for two case studies. In these simulations, the reference voltage $V^{\text{ref}}_k = 1$ p.u. and $\sigma = 5$; the

[2]This model is known as Type DC1A excitation system [39], and is adopted here for illustration purposes only. Any applicable exciter model may be used instead.

[3]The dynamics of the voltage sensing subsystems have been neglected, being relatively fast.

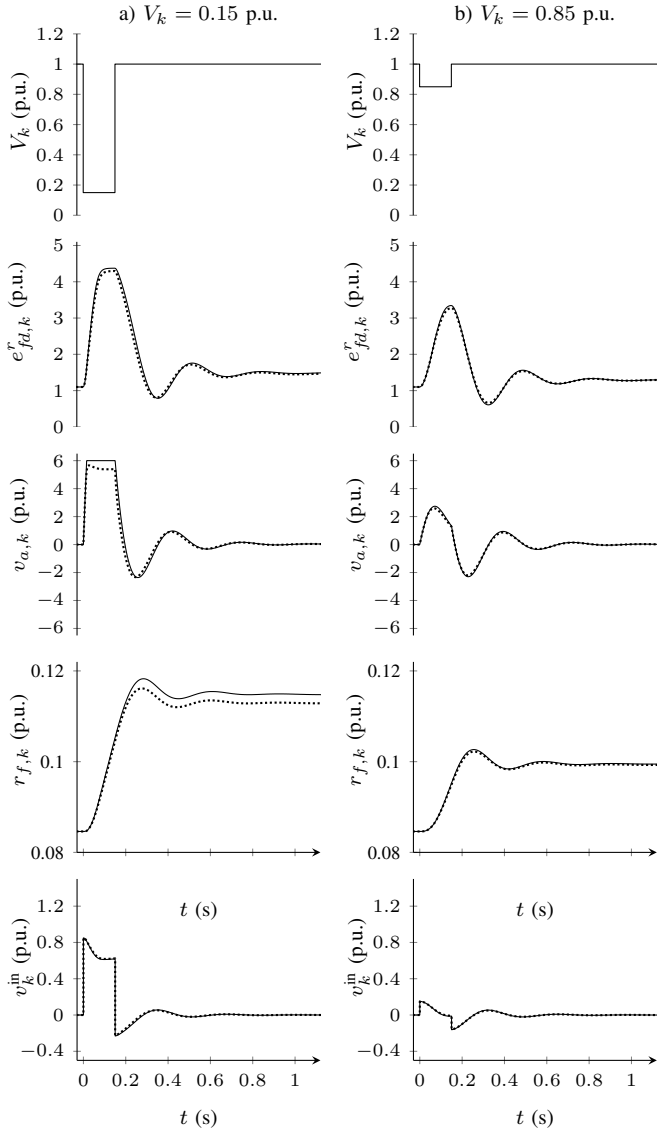


Fig. 1. Response of an excitation system to two voltage dips at $t = 0$ s which yield terminal voltages $V_k = 0.15$ p.u. and $V_k = 0.85$ p.u. that last 9 cycles of 60 Hz. The dotted and solid traces correspond to models of the voltage amplifier with a smooth saturation function and hard limits, respectively.

exciter parameters are obtained from Table I of Section V for $k = 1$. The selected voltage sags, where $V_k = 0.15$ and $V_k = 0.85$ p.u., could be representative of transmission faults that occur relatively close and far from the terminals of a synchronous generator, respectively. The main variable of interest in a transient stability study is the excitation voltage $e_{fd,k}$. The comparison of the two modeling approaches shows acceptable performance, while maintaining the amplifier voltage saturated within desired limits. The adopted saturation model is convenient from an application perspective, because it facilitates the Taylor polynomial-based Picard iterations of (6).

### C. Loads, Renewable Generation, and Transmission Network

During the first swing, loads are assumed to behave as constant impedances [5]. On the other hand, renewable generation injects zero active and nonzero reactive power [41]. Here, for illustration purposes, the control strategy of the $h^{\text{th}}$ renewable power plant ($h = 1, \ldots, m$) is to supply reactive power according to the equation[4]

$$Q_h = B_{C,h} V_h^2 \tag{20}$$

with $V_h$ the voltage magnitude at the terminals of the power plant and $B_{C,h}$ some prescribed constant.

The network seen by the synchronous generators (comprising loads, renewable generation response, and transmission system) can be represented in quasi steady state by phasor equations

$$\tilde{I}_{as} = Y_\gamma \tilde{E}_{as} \tag{21}$$

where $Y_\gamma \in \mathbb{C}^{n\times n}$ is a reduced complex admittance matrix [5]. The vectors $\tilde{I}_{as}$ and $\tilde{E}_{as} \in \mathbb{C}^n$ contain all generator current and voltage phasors, respectively. Two versions of $Y_\gamma$ for $\gamma \in \{1, 2\}$ represent the transmission system during the fault and after it has been cleared, respectively. The fault is cleared after a prescribed time $t_c$ by protective devices.

Using *qd* variables in a common synchronous reference frame (denoted by a superscript '$e$') so that $\tilde{F}_{as} = f_q^e - j f_d^e$ [42], (21) can be rewritten by equating real and imaginary parts as

$$I^e = S_\gamma E^e \tag{22}$$

where $F^e = (f_{qd,1}^{eT}, \ldots, f_{qd,n}^{eT})^T \in \mathbb{R}^{2n\times 1}$ and $S_\gamma \in \mathbb{R}^{2n\times 2n}$. Generator variables are mapped from the individual rotor reference frames to the common synchronous reference frame by [42]

$$f_{qd,k}^e = \begin{pmatrix} \cos\theta_k & \sin\theta_k \\ -\sin\theta_k & \cos\theta_k \end{pmatrix} f_{qd,k}^r = T(\theta_k) f_{qd,k}^r \,. \tag{23}$$

Hence, (22) becomes

$$K(\theta) I^r = S_\gamma K(\theta) E^r \tag{24}$$

where $K(\theta) = \text{Diag}(T(\theta_1), \ldots, T(\theta_n)) \in \mathbb{R}^{2n\times 2n}$ is block diagonal, $F^r = (f_{qd,1}^{rT}, \ldots, f_{qd,n}^{rT})^T \in \mathbb{R}^{2n\times 1}$, and $\theta = (\theta_1, \ldots, \theta_n)^T \in \mathbb{R}^n$. Premultiplying both sides of (24) by $\text{Diag}(T^T(\theta_1), \ldots, T^T(\theta_1)) \in \mathbb{R}^{2n\times 2n}$ yields, after some elementary matrix algebra,

$$I^r = K^T(\delta) S_\gamma K(\delta) E^r = R_\gamma(\delta) E^r \tag{25}$$

with $\delta = (0, \delta_{2,1}, \ldots, \delta_{n,1})^T \in \mathbb{R}^n$. That is, a new matrix $R_\gamma(\delta) \in \mathbb{R}^{2n\times 2n}$ has been introduced, where rotor angles are referred to $\theta_1$.[5]

### D. Interconnected Power System

The collection of the ODEs (8), (9), (10), (12), (13), and (14) for $k = 1, \ldots, n$, together with the algebraic equa-

[4] It is certainly possible to model more advanced reactive power compensation schemes by power electronic converter-interfaced renewables, but this is outside the scope of the present study.

[5] When interconnecting the generators in the system study, $f_{qd,k}^r$ in (9) is selected from $F^r$ via $f_{qd,k}^r = C_k F^r$ with $C_k \in \mathbb{R}^{2\times 2n}$.

tion (25), yield a system as in (1)-(2),[6] where

$$z = (E^{rT}, \omega^T, \delta^T, e_{fd}^{rT}, r_f^T, v_a^T)^T \in \mathbb{R}^{7n-1} \tag{26}$$

$$u = T_m \in \mathbb{R}^n \tag{27}$$

are state and input vectors, respectively. The vectors $\omega^T = (\omega_1, \ldots, \omega_n)$ and $T_m^T = (T_{m,1}, \ldots, T_{m,n})$ are introduced for notational convenience. The selected system outputs for transient stability assessment are[7]

$$w = (V^T, \Omega^T, \delta^T, e_{fd}^{rT}, v_a^T)^T \in \mathbb{R}^{5n-2}\,. \tag{28}$$

$V^T = (V_1, \ldots, V_n)$ is a vector of terminal voltages (16), and $\Omega^T = (\omega_{2,1}, \ldots, \omega_{n,1})$ with $\omega_{k,1} = \omega_b(\omega_k - \omega_1)$ represents the relative rotor speed of (10). Since the network topology is switched at a prescribed moment in time, the voltage outputs are discontinuous.

### *E. Polynomials of Initial Conditions and Inputs*

The uncertain initial conditions and inputs (states and prime mover torques of each synchronous machine) are initialized from an uncertain power flow, where the uncertainty stems from the renewable power injection. Recall that we have $n$ conventional (dispatchable) and $m$ renewable generators. Their powers are placed in the vector

$$P = (P_1, \ldots, P_k, \ldots, P_n, \ldots, P_{n+h}, \ldots, P_{n+m})^T\,. \tag{29}$$

For simplicity, assume that the renewables are not correlated.

Consider an uncertain renewable source (element $q > n$ of above vector) with uncertain power output $P_{q0} + [-1, 1]\Delta P_q$, with $\Delta P_q > 0$ the radius of the uncertainty. The impact of this uncertain generation can be absorbed by the remaining dispatchable generators using pre-specified (by the system operator) participation factors. This is modeled with a vector $P_i$ where: its $q$-th element is equal to $\Delta P_q$; $P_{i,j} = 0$, $j > n$, $j \neq q$; and $\sum_j P_{i,j} = 0$.[8] Considering all $n_p \leq m$ renewable uncertainties leads to

$$P(p) = P_0 + \sum_{i=1}^{n_p} p_i P_i \tag{30}$$

The vector $P_0$ represents a nominal dispatch of the power system, which is obtained using an ac power flow. Recall from Section II that the polynomial variables $p_i \in [-1, 1]$.

Uncertain power generation can be related to the terminal voltage angles of all $n + m$ units by [7]:

$$\Delta P(p) = B\Delta\varphi(p) \tag{31}$$

where $\Delta P(p) = P(p) - P_0$ and $B \in \mathbb{R}^{(m+n)\times(m+n)}$ is a reduced network susceptance matrix from a dc power flow formulation. By solving (31) for $\Delta\varphi(p)$, a polynomial vector of uncertain voltage angles at the terminals of conventional and renewable generators is

$$\varphi(p) = \varphi_0 + \Delta\varphi(p)\,. \tag{32}$$

Here, $\varphi_0$ is obtained from the ac power flow solution based on $P_0$. Notice that $\varphi_1(p) = \Delta\varphi_1(p) = 0$ in $\varphi(p)$ of (32), representing the reference bus voltage angle. We assume that the reactive power supplied by the synchronous machines is unaffected by the active-power variability of renewables, hence

$$Q_k(p) = Q_{0,k} \tag{33}$$

where $Q_0$ is obtained from the ac power flow solution based on $P_0$. The initial conditions $z_0(p)$ and inputs $u(p)$ are obtained by performing function compositions with polynomials. In particular, the operations are replaced with appropriate $n_d$-order Taylor expansions, which are given in Appendix A.

The initialization proceeds as follows:

1) Compute real and imaginary components of the voltage phasor $\tilde{V}_k(p)$:

$$V_k^{\text{re}}(p) = V_k c_{\varphi,k}(p) \tag{34}$$

$$V_k^{\text{im}}(p) = V_k s_{\varphi,k}(p) \tag{35}$$

where $V_k = V_k^{\text{ref}}$ at $t = 0$ (terminal voltage equals its reference) and

$$c_{\varphi,k}(p) \approx \cos(\varphi_k(p)) \tag{36}$$

$$s_{\varphi,k}(p) \approx \sin(\varphi_k(p)) \tag{37}$$

are trigonometric function compositions of $\varphi_k(p)$.

2) Compute real and imaginary components of the current phasor $\tilde{I}_k(p)$ using (30) and (33):

$$I_k^{\text{re}}(p) \approx \frac{1}{V_k}\left(P_k(p)c_{\varphi,k}(p) + Q_k(p)s_{\varphi,k}(p)\right) \tag{38}$$

$$I_k^{\text{im}}(p) \approx \frac{1}{V_k}\left(P_k(p)s_{\varphi,k}(p) - Q_k(p)c_{\varphi,k}(p)\right)\,. \tag{39}$$

3) Calculate cosine and sine (not the angle itself) of the rotor angle position:

$$c_{\theta,k}(p) \approx U_k^{\text{re}}(p)\frac{1}{U_k(p)} \tag{40}$$

$$s_{\theta,k}(p) \approx U_k^{\text{im}}(p)\frac{1}{U_k(p)} \tag{41}$$

where

$$U_k^{\text{re}}(p) = V_k^{\text{re}}(p) - X_{q,k}I_k^{\text{im}}(p) \tag{42}$$

$$U_k^{\text{im}}(p) = V_k^{\text{im}}(p) + X_{q,k}I_k^{\text{re}}(p) \tag{43}$$

$$U_k(p) \approx \sqrt{U_k^{\text{re}^2}(p) + U_k^{\text{im}^2}(p)}\,. \tag{44}$$

4) Compute *qd* terminal voltages and currents in the rotor reference frame:

$$v_{q,k}^r(p) \approx V_k^{\text{re}}(p)c_{\theta,k}(p) + V_k^{\text{im}}(p)s_{\theta,k}(p) \tag{45}$$

$$v_{d,k}^r(p) \approx V_k^{\text{re}}(p)s_{\theta,k}(p) - V_k^{\text{im}}(p)c_{\theta,k}(p) \tag{46}$$

[6]Notice in (25) that $I^r$ (vector of algebraic variables) are explicit functions of $\delta$ and $E^r$ (vectors of state variables), hence the algebraic variables $i_{qd,k}^r$ of (8) and (9) can be written as a function of the states, leading to an ODE.

[7]Outputs can be specified for analysis purposes and/or to represent measurable variables from the system.

[8]Uncertain generation also yields uncertain transmission power losses. These losses are neglected.

$$i^r_{q,k}(p) \approx I^{\text{re}}_k(p) c_{\theta,k}(p) + I^{\text{im}}_k(p) s_{\theta,k}(p) \tag{47}$$

$$i^r_{d,k}(p) \approx I^{\text{re}}_k(p) s_{\theta,k}(p) - I^{\text{im}}_k(p) c_{\theta,k}(p)\,. \tag{48}$$

5) Compute initial conditions and torque input of the synchronous generators:[9]

$$e^r_{q,k}(p) = v^r_{q,k}(p) + X'_{d,k} i^r_{d,k}(p) \tag{49}$$

$$e^r_{d,k}(p) = v^r_{d,k}(p) - X'_{q,k} i^r_{q,k}(p) \tag{50}$$

$$T_{m,k}(p) \approx e^r_{q,k}(p) i^r_{q,k}(p) + e^r_{d,k}(p) i^r_{d,k}(p)\,. \tag{51}$$

6) Assign the polynomial representing rotor speed:

$$\omega_{k0}(p) = 1\,. \tag{52}$$

7) Compute the rotor angle position

$$\theta_k(p) \approx \operatorname{asin}\left(s_{\theta,k}(p)\right) \tag{53}$$

with $s_{\theta,k}(p)$ from (41).

8) Calculate relative rotor angles:

$$\delta_{k,1}(p) = \theta_k(p) - \theta_1(p) \tag{54}$$

for all $k = 2, \ldots, n$.

9) Compute the initial conditions of the excitation system:

$$e^r_{fd,k}(p) = e^r_{q,k}(p) + \left(X_{d,k} - X'_{d,k}\right) i^r_{d,k}(p) \tag{55}$$

$$r_{f,k}(p) = \frac{K_{F,k}}{T_{F,k}} e^r_{fd,k0}(p) \tag{56}$$

$$v_{a,k}(p) = 0\,. \tag{57}$$

10) Calculate the functional dependence of the initial condition-dependent parameter [see (12)] on $p$:

$$K_{E,k}(p) \approx -S_{E,k}\left(e^r_{fd,k}(p)\right)\,. \tag{58}$$

The polynomial $z_0(p)$ is assembled by collecting (49), (50), (52), (54), (55), (56), and (57) in a vector as in (26). The input vector $u(p)$ is assembled by the polynomials of (51). The parameter (58) is used in (12).

## IV. First-Swing Transient Stability Assessment

Transient stability is studied using Algorithm 1, whose main steps are outlined here. The parameters of all synchronous generators and excitation subsystems (e.g., time constants and reactances) are embedded within a data structure *GE*, which is passed as a parameter to the algorithm among other necessary pieces of information, such as the network matrices $S_\gamma$.

The algorithm begins by calculating polynomials at $t = 0$, namely, $z_0(p)$ and $u(p)$ that describe uncertain initial conditions and inputs, respectively, using the steps of Section III-E. In line 2, the corresponding system output polynomial $w_0(p)$ is calculated. In line 3, an interval vector that contains the set of system outputs at $t = 0$ is computed (for plotting) as explained in Appendix C.

[9]Since stator ohmic losses are neglected, the coefficients of the monomials of $T_{m,k}(p)$ should be relatively similar to those of $P_k(p)$ of (30) ($k = 1, \ldots, n$). This fact could be used to assert whether the initialization is correct.

**Algorithm 1:** Transient Stability Assessment

**Data**: Total number of steps $s_n$, elapsed number of steps to clear the fault $s_c$, time step $r$, set of network matrices $\{S_1, S_2\}$, generator and excitation system parameters *GE*, polynomial of power generation $P(p)$, polynomial degree $n_d$.

**Result**: System output polynomials $w_s(p)$ and intervals $[\underline{w}_s, \overline{w}_s]$ for $s = 0, 1, \ldots, s_n$, and first-swing stability diagnosis $D \in \{\text{'stable'}, \text{'unstable'}\}$.

1 $z_0(p), u(p) \leftarrow \texttt{initialization}(P(p), \textit{GE})$
2 $w_0(p) \leftarrow \texttt{outputs}(z_0(p), \textit{GE}, S_1)$
3 $\underline{w}_0, \overline{w}_0 \leftarrow \texttt{interval}(w_0(p))$
4 $t_0 \leftarrow 0$
5 **for** $s = 1$ **to** $s_n$ **do**
6 $\quad \gamma \leftarrow \texttt{switch}(s, s_c)$
7 $\quad z_s(p) \leftarrow \texttt{Picard}(z_{s-1}(p), u(p), \textit{GE}, S_\gamma, r, n_d)$
8 $\quad w_s(p) \leftarrow \texttt{outputs}(z_s(p), \textit{GE}, S_\gamma)$
9 $\quad \underline{w}_s, \overline{w}_s \leftarrow \texttt{interval}(w_s(p))$
10 $\quad t_s \leftarrow t_{s-1} + r$
11 **end**
12 $D \leftarrow \texttt{assessment}(\{[\underline{w}_s, \overline{w}_s] : s = s_c, \ldots, s_n\})$

The operations of the main loop start in line 6 by choosing the index

$$\gamma = \begin{cases} 1 & \text{if } s \le s_c \ \ \text{(during the fault)} \\ 2 & \text{if } s > s_c \ \ \text{(after the fault is cleared)} \end{cases} \tag{59}$$

that selects the appropriate network matrix $S_\gamma$ for the $s$-th time interval. Recall that $s_c$ of (59) indicates the time $t_c = s_c r$ for which the fault remains active. In line 7, the state polynomial $z_s(p)$ is computed using Picard iterations, as explained in Section II. In line 8, the output polynomial $w_s(p)$ (defined in (28)) is calculated. In line 9, an interval vector containing the outputs is obtained.

In line 12, the determination of (first-swing) transient stability takes place. This is based on the lower and upper bounds of the relative rotor speed interval vectors, $[\underline{\Omega}_s, \overline{\Omega}_s]$, for $s = s_c + 1, \ldots, s_n$, which are extracted from the output vector. This range of $s$ is chosen because we are interested in the first-swing stability of the system after the fault is cleared.

*Definition 1:* A relative rotor angle is said to "swing" when a maximum or minimum is reached as time progresses.

Based on the above definition, the assessment is performed by checking for relative rotor speed zero crossings as follows. Let the interval $[\underline{\Omega}_{s,l}, \overline{\Omega}_{s,l}]$ be the $l^{\text{th}}$ entry of $[\underline{\Omega}_s, \overline{\Omega}_s]$, with $l = 1, \ldots, n-1$ (there are $n-1$ relative rotor speeds). The power system is considered first-swing stable if there exist indexes $\alpha_l,\ \beta_l \in \{s_c, \ldots, s_n\}$ such that

$$\underline{\Omega}_{\alpha_l,l} \cdot \underline{\Omega}_{\alpha_l+1,l} < 0 \tag{60}$$

and

$$\overline{\Omega}_{\beta_l,l} \cdot \overline{\Omega}_{\beta_l+1,l} < 0 \tag{61}$$

for all $l = 1, \ldots, n-1$; otherwise, the power system is

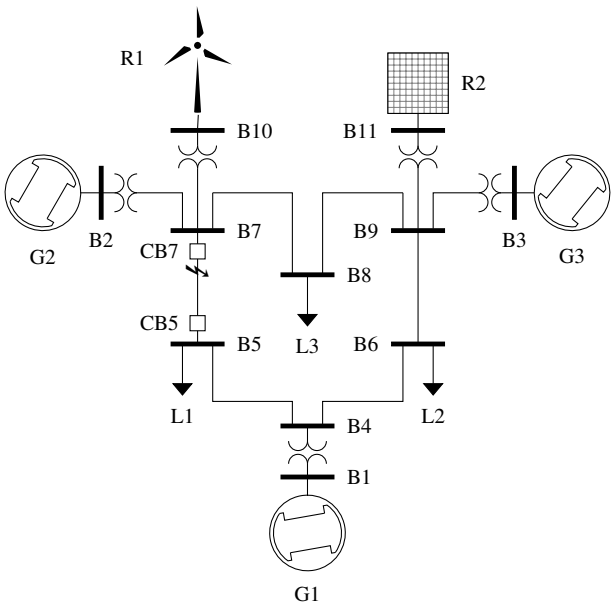


Fig. 2. Modified WSCC nine-bus power system.

TABLE I
TYPE DC1A EXCITATION SYSTEM PARAMETERS

| $k$ | $T_{E,k}$ | $A_{E,k}$ | $B_{E,k}$ | $K_{F,k}$ | $T_{F,k}$ | $K_{A,k}$ | $T_{A,k}$ | $V_{A,k}^{\lim}$ |
|---|---|---|---|---|---|---|---|---|
| 1 | 0.1 | $9.6{\cdot}10^{-3}$ | 1.14 | 0.1 | 1.3 | 50 | 0.1 | 6.0 |
| 2 | 0.57 | $1.3{\cdot}10^{-3}$ | 1.37 | 0.09 | 0.35 | 20 | 0.4 | 2.0 |
| 3 | 0.68 | $1.6{\cdot}10^{-3}$ | 1.63 | 0.11 | 0.35 | 15 | 0.3 | 1.0 |

unstable. In view of (10), the $l$-th pair indicates whether or not all possible trajectories of the $l^{\text{th}}$ relative rotor angle will exhibit a swing.

As a post-processing stage of Algorithm 1 (not explicitly shown), one can generate one or more particular trajectories using the sequence of output polynomials. This is accomplished by evaluating $w_s(p)$ ($s = 0, 1, \ldots, s_n$) for given $p$ that represents the level of renewable generation at the moment of the fault.

## V. CASE STUDIES

We study a modified WSCC nine-bus power system, shown in Fig. 2. This system has $n = 3$ synchronous generators. The parameters of the WSCC power system are specified in [5, Table 2.1], given in per unit (p.u.) on a common 100-MVA power base. The excitation system parameters are specified in Table I, which are obtained from [5, Appendix D]. The amplifier state saturation function of (19) uses $\sigma = 5$. Two renewable power sources (i.e., $m = 2$), namely R1 and R2, have been integrated to the system by means of two step-up transformers, each rated for 50 MVA and having an impedance value of 8% on the 50-MVA base. The loads are considered to be known without uncertainty, and are modeled as constant impedances during the transient.

Two studies are considered to show first-swing transient stability and instability. In both cases, the power system is perturbed by a three-phase fault that occurs on the transmission line 5-7 at a point that is next to bus B7 (see Fig. 2). The fault is cleared by opening the circuit breakers CB5 and CB7 in 5 cycles. During the first-swing time horizon, the two renewable power plants are programmed to supply reactive power resembling capacitive reactances with $B_{C,1} = 0.5$ p.u. and $B_{C,2} = 0.5$ p.u. [see (20)].

The studies were conducted on a 2.2-GHz Intel Core i7 personal computer. All polynomial operations were implemented using standard matrix computations and object-oriented programming in Matlab 2015a [43]. The parameters considered in Algorithm 1 are $r = 1/120$ s, $n_d = 6$, $s_c = 10$, and $s_n = 134$. The CPU time to run each case study was approximately 27 s. The uncertain dispatch conditions are calculated by considering 0.24 p.u. power uncertainty in each renewable power source, i.e., $\Delta P_q = 0.12$ p.u. ($q \in \{4, 5\}$). This means that we consider a total uncertainty of $0.48$ p.u. in a power system that supplies a total demand of $3.15$ p.u.

In particular, the polynomial (30) for the stable case study is obtained from the results of a power flow

$$P_0 = (0.891, 1.4, 0.4, 0.25, 0.25)^T \tag{62}$$

and arbitrarily selected participation factor vectors

$$P_1 = 0.12 \cdot (-0.3, -0.4, -0.3, 1, 0)^T \tag{63}$$

$$P_2 = 0.12 \cdot (-0.3, -0.4, -0.3, 0, 1)^T . \tag{64}$$

Here, $p = (p_1,\ p_2)^T$. The two sources of uncertainty from the renewable power sources are distributed among the synchronous generators as described in Section III-E. To yield the unstable case, we use the following power flow result

$$P_0 = (0.892, 1.62, 0.44, 0.12, 0.12)^T \tag{65}$$

and the same vectors of (63) and (64). Substitution of (62)–(64) in (30) yields, for example, $P_4(p) = 0.25 + 0.12p_1$ with $p_1 \in [-1, 1]$, which implies that $P_4(p) \in [0.13, 0.37]$ p.u.

Results of system outputs showing first-swing transient stability and instability are illustrated in Figs. 3–5. Time-domain intervals, deterministic trajectories, and polynomial-based trajectories are displayed using gray, solid-black, and dotted-black traces, respectively. The time domain intervals are obtained from $[\underline{w}_s, \overline{w}_s]$ for $s = 0, 1, \ldots, s_n$, which is an output of Algorithm 1. The deterministic trajectories are generated using the analytic model of Section III and a numerical ODE solver (viz., ode23s in Matlab, with a maximum step size of $1/300$ s), whose initial conditions are obtained by evaluating $z_0(p)$ at the following points:

$$p \in \left\{(0,0)^T,\ (1,1)^T,\ (-1,0)^T,\ (-1,-1)^T\right\} . \tag{66}$$

The polynomial-based trajectories are obtained by evaluating the sequence $w_s(p)$ for $s = 0, 1, \ldots$ from Algorithm 1 at the same values of (66). It is interesting to note that even the extreme points, where $|p_j| = 1$ and the approximation error is greatest, yield acceptable results.

The polynomial-based trajectories have been down-sampled in the plots for visibility. Note that in Figs. 3–5 the deter-

ministic and polynomial-based trajectories are in agreement among each other. This implies that the Picard iterations of Algorithm 1 provided satisfactory results for first-swing transient stability assessment.

Figure 3 shows time-domain intervals of stable and unstable relative rotor angles and speeds. In the stable case, both upper and lower bounds of all relative speeds ($\omega_{2,1}$ and $\omega_{3,1}$) cross zero. However, in the unstable case, the upper bounds of the relative speeds do not cross zero; hence, a subset of the trajectories of relative rotor angles may diverge, which implies loss of synchronism among generators. It is interesting to observe in the unstable case that the set of initial conditions yields both stable and unstable trajectories, which the method can produce without any particular difficulty. The simulations showing the unstable case were stopped early (i.e., once the uncertainty of any relative rotor angle exceeds $150°$), since the order of the Taylor polynomials used in this study is deemed insufficient in view of (72) and (73) for $n_d = 6$.

Figures 4 and 5 illustrate time-domain intervals of generator terminal voltages and their excitation controls for the stable and unstable cases. These outputs are plotted for informative purposes only, as they are not used in establishing first-swing stability.

## VI. Conclusion

This paper has set forth a method to study first-swing rotor angle stability of power systems in the context of renewable power generation uncertainty. Due to its generality, the proposed method can incorporate arbitrary nonlinear exciter (and other component) models, thereby offering excellent accuracy. An important contribution of this work is the calculation of the effect of renewable power generation uncertainty on initial conditions and system inputs. All calculations are based on multivariate polynomials, which also facilitate the numerical solution of the underlying nonlinear ordinary differential equations, which is obtained using Picard iterations. Transient stability is assessed through an examination of the time-domain intervals of rotor speeds.

The method was tested successfully on a small power system example. However, further application to large-scale power system models is necessary; this remains under investigation. Also, it is the authors' opinion that an important enhancement of the algorithm would be its extension for handling power systems modeled with differential algebraic equations. Such capability would permit incorporation of more complex load models, such as voltage- or frequency-dependent loads, or loads that withdraw constant power and/or current.

## Appendix A
## Taylor Series Expansions

Let $z,\ z_c \in \mathbb{R}$ represent a function variable and an expansion center, respectively. Here, these variables are polynomials of $p$, and we have $z = z(p)$ and $z_c = z(0)$. The calculation of some nonlinear expressions that commonly appear in the transient stability model equations is performed as follows:

$$\sin z \approx \sin z_c \cdot \mathtt{tcos}\,(z - z_c) + \cos z_c \cdot \mathtt{tsin}\,(z - z_c) \quad (67)$$

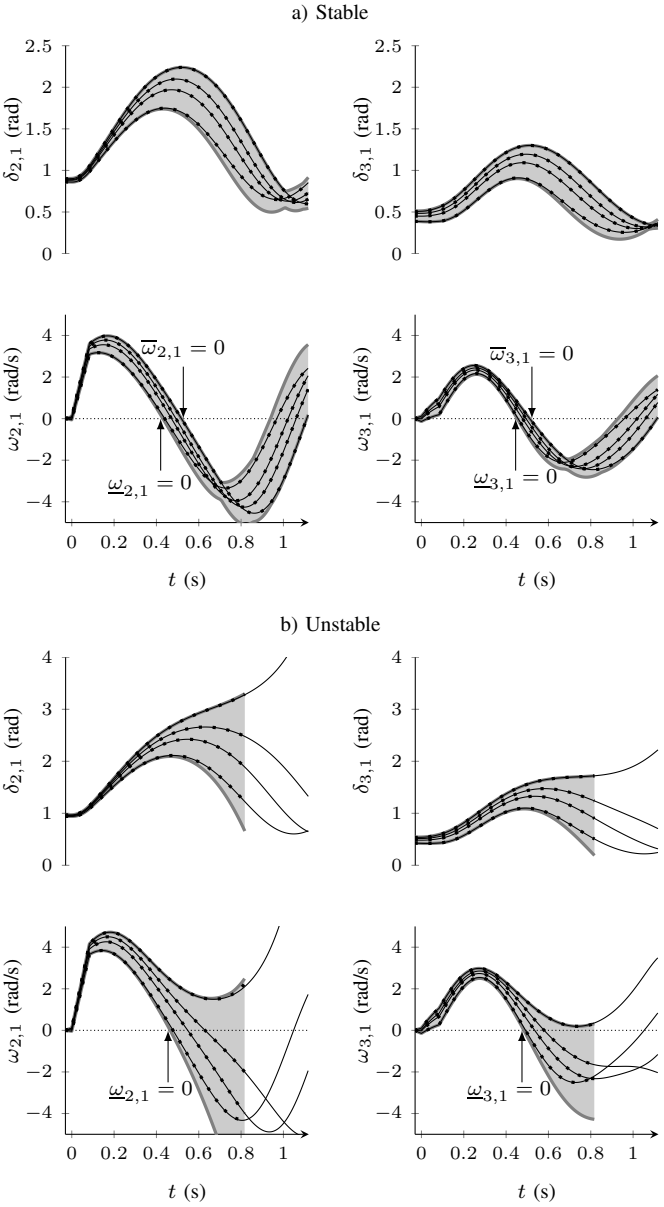


Fig. 3. Stable and unstable relative rotor angle and relative speed bounds (gray), deterministic trajectories (solid black), and polynomial-based trajectories (dotted black).

$$\cos z \approx \cos z_c \cdot \mathtt{tcos}\,(z - z_c) - \sin z_c \cdot \mathtt{tsin}\,(z - z_c) \quad (68)$$

$$e^z \approx e^{z_c} \cdot \mathtt{texp}\,(z - z_c) \quad (69)$$

$$\sqrt{z} \approx \sqrt{z_c} \cdot \mathtt{tsqrt}\left(1 + \frac{z - z_c}{z_c}\right),\ z_c > 0 \quad (70)$$

$$\frac{1}{z} \approx \frac{1}{z_c} \cdot \mathtt{tinv}\left(1 + \frac{z - z_c}{z_c}\right),\ z_c \neq 0 \quad (71)$$

where the following Taylor expansions are used (up to order $n_d$)

$$\mathtt{tsin}\,(\eta) = \sum_{i=1}^{\lceil \frac{n_d}{2} \rceil} \frac{(-1)^{i-1}}{(2i-1)!} \cdot \eta^{2i-1} \quad (72)$$

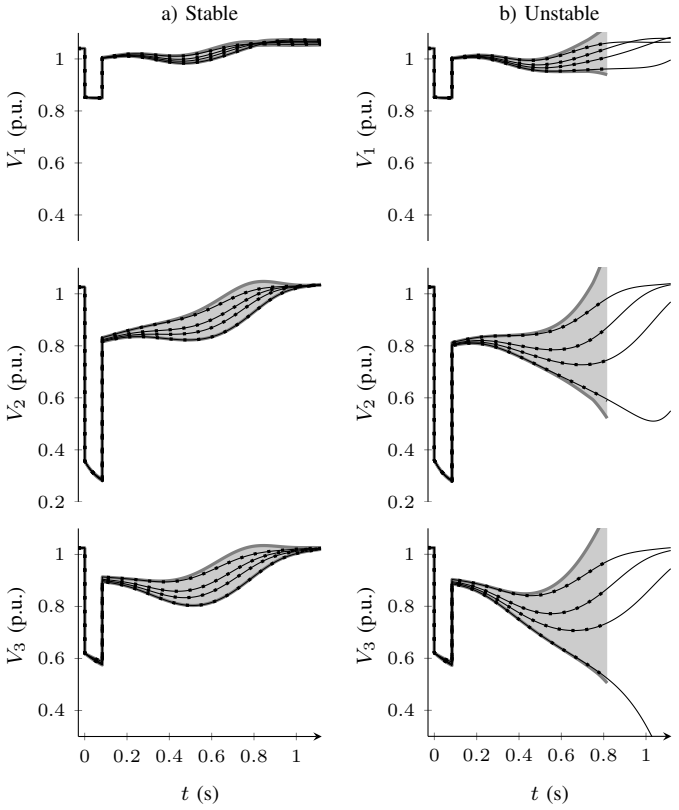


Fig. 4. Stable and unstable terminal voltage bounds (gray), deterministic trajectories (solid black), and polynomial-based trajectories (dotted black).

$$\texttt{tcos}\,(\eta) = 1 + \sum_{i=1}^{\lceil \frac{n_d}{2} \rceil} \frac{(-1)^i}{(2i)!} \cdot \eta^{2i} \tag{73}$$

$$\texttt{texp}\,(\eta) = 1 + \sum_{i=1}^{n_d} \frac{1}{i!} \cdot \eta^{i} \tag{74}$$

$$\texttt{tsqrt}\,(1+\eta) = 1 + \sum_{i=1}^{n_d} \frac{(-1)^i (2i)!}{4^i (i!)^2 (1-2i)} \cdot \eta^{i},\ \eta \geq -1 \tag{75}$$

$$\texttt{tinv}\,(1+\eta) = 1 + \sum_{i=1}^{n_d} (-1)^i \cdot \eta^{i},\ |\eta| < 1\,. \tag{76}$$

In addition, we use the following series for $|z| \leq 1$:

$$\text{asin}(z) \approx \texttt{tasin}(z) = \sum_{i=0}^{\lfloor \frac{n_d}{2} \rfloor} \frac{4^{-i}}{2i+1} \binom{2i}{i} \cdot z^{2i+1}\,. \tag{77}$$

## Appendix B
## Example of Picard Iterations

This example illustrates the use of Picard iterations to approximate the solution of the ODE

$$\frac{dz}{dt} = F(z,u) = -\sin z + u \tag{78}$$

with initial condition set

$$\mathcal{Z}_0 = \left\{ z_0(p_1) = \frac{\pi}{2} + 0.1 p_1 : p_1 \in [-1,1] \right\} \tag{79}$$

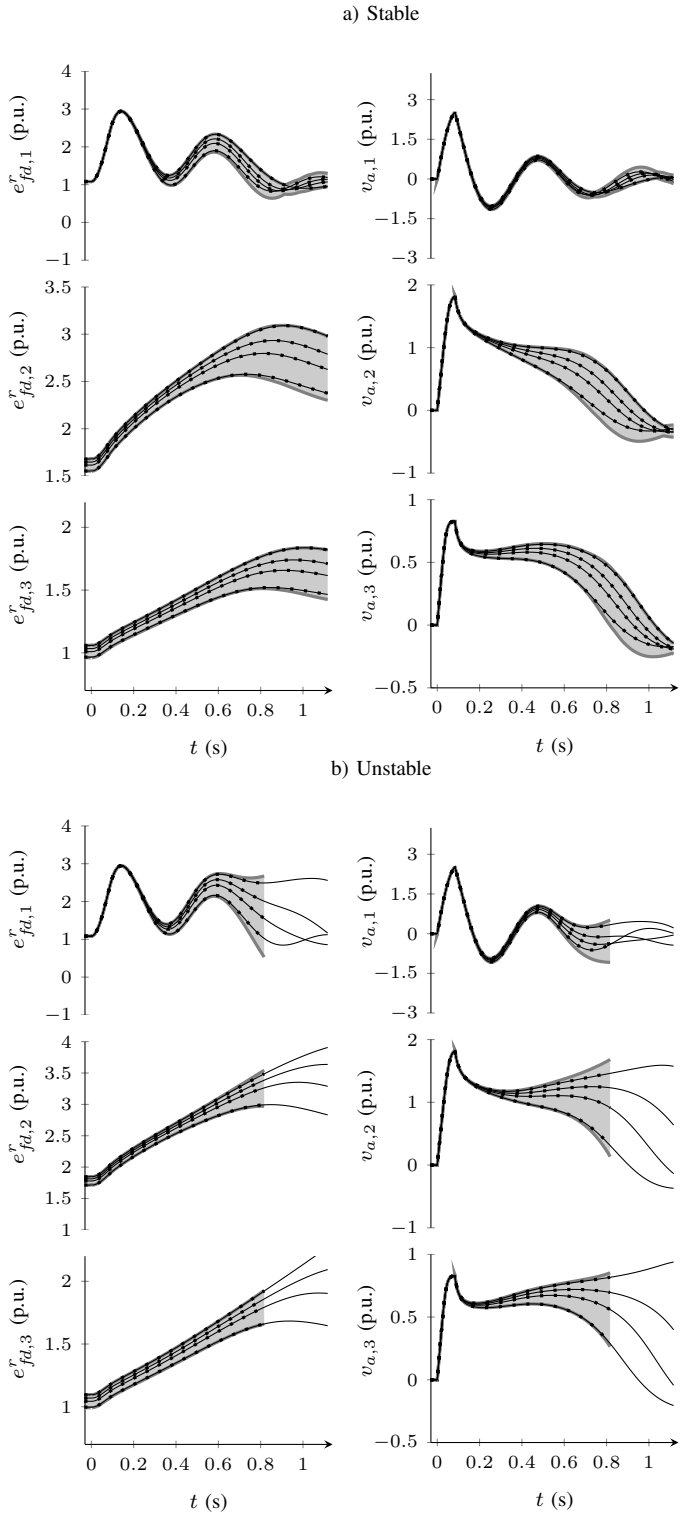


Fig. 5. Stable and unstable excitation system bounds (gray), deterministic trajectories (solid black), and polynomial trajectories (dotted black).

and input set

$$\mathcal{U} = \{ u(p_2) = 1 + 0.1 p_2 : p_2 \in [-1,1] \}\,. \tag{80}$$

The previous ODE and sets of initial conditions and inputs have no physical significance; they were conceived to illustrate the Picard iterative process in a relatively simple manner.

In this example, we calculate the polynomial $z_1(p) = z_1(p_1, p_2)$ that represents the set of states

$$\mathcal{Z}_1 = \{z_1(p) : p_j \in [-1, 1],\, j = 1, 2\} \tag{81}$$

of the ODE (78) at $t = r = 1$. We consider Taylor polynomial expansions and multivariate polynomials of fourth degree ($n_d = 4$) in the calculations. Higher-order terms are dropped, similarly to how they would be implemented in a computer program and stored in memory.

The algorithm proceeds as follows:

1) The fourth-degree Taylor expansion of $F$ is obtained:

$$\begin{aligned} F(z,u) =& -\sin z_c \cos(z - z_c) \\ & - \cos z_c \sin(z - z_c) + u_c + (u - u_c) \\ \approx& -\sin z_c \left(1 - \frac{(z-z_c)^2}{2} + \frac{(z-z_c)^4}{24}\right) \\ & - \cos z_c \left((z - z_c) - \frac{(z-z_c)^3}{6}\right) \\ & + u_c + (u - u_c)\,. \end{aligned} \tag{82}$$

   Please see Appendix A for details on Taylor expansions. Let $(z_c, u_c) = (z_0(0), u(0)) = (\pi/2, 1)$. Hence,

$$F(z,u) \approx \frac{(z-\pi/2)^2}{2} - \frac{(z-\pi/2)^4}{24} + (u - 1)\,. \tag{83}$$

   In this example, $F(z_c, u_c) = 0$ for simplicity, but this condition does not need to hold in general.

2) The Picard iterations are initialized by setting

$$\zeta_1^{(0)}(p,\tau) = z_0(p) = \frac{\pi}{2} + 0.1p_1 + 0p_2 + 0\tau\,. \tag{84}$$

   Here, time $\tau$ is introduced as an extra monomial variable (hence, the total number of variables $n_p = 3$). Note that $p_2$ and $\tau$ are explicitly listed with zero coefficients. Recall from Section II that we consider (for implementation purposes) that all possible monomials are present. The other higher-order zero-coefficient monomials, which are part of the fourth-order polynomial on $p_1$, $p_2$, and $\tau$, are not shown.

3) The polynomial

$$\begin{aligned} \mathsf{F}_1^{(0)}(p,\tau) &= F\left(\zeta_1^{(0)}(p,\tau), u(p_2)\right) \\ &= 0.1p_2 + 0.005p_1^2 - 4.17\cdot 10^{-6}p_1^4 + 0\tau \end{aligned} \tag{85}$$

   is calculated using (83).

4) A Picard iteration is performed,

$$\begin{aligned} \zeta_1^{(1)}(p,\tau) &= z_0(p) + \int_0^\tau \mathsf{F}_1^{(0)}(p,\mu)\, d\mu \\ &\approx \frac{\pi}{2} + 0.1p_1 + 0.1p_2\tau + 0.005p_1^2\tau \end{aligned} \tag{86}$$

   using $\mathsf{F}_1^{(0)}(p,\tau)$ of step 3. Note that the resulting polynomial of this step has been truncated to maintain a fourth-order polynomial representation. Otherwise, a fifth order polynomial due to the monomial $p_1^4\tau$ would have been obtained.

5) Steps 3–5 are repeated using the latest polynomial $\zeta_1^{(v-1)}(p,\tau)$ with $v \in \{2, 3, 4\}$ [see (6)]. At most $n_d = 4$ Picard iterations are necessary to generate the desired degree polynomial solution on $p_1$, $p_2$, and $\tau$ [44]. For example, steps 3 and 4 in the next iterations yield the following polynomials:

$$\begin{aligned} \mathsf{F}_1^{(1)}(p,\tau) &= 0.1p_2 + 5\cdot 10^{-3}p_1^2 + 0.01p_1p_2\tau \\ &- 4.17\cdot 10^{-6}p_1^4 + 5\cdot 10^{-4}p_1^3\tau + 5\cdot 10^{-3}p_2^2\tau^2 \end{aligned} \tag{87}$$

$$\begin{aligned} \zeta_1^{(2)}(p,\tau) &= \frac{\pi}{2} + 0.1p_1 + 0.1p_2\tau \\ &+ 5\cdot 10^{-3}p_1^2\tau + 5\cdot 10^{-3}p_1p_2\tau^2 \end{aligned} \tag{88}$$

$$\begin{aligned} \mathsf{F}_1^{(2)}(p,\tau) &= 0.1p_2 + 5\cdot 10^{-3}p_1^2 + 0.01p_1p_2\tau \\ &- 4.17\cdot 10^{-6}p_1^4 + 5\cdot 10^{-4}p_1^3\tau + 5\cdot 10^{-3}p_2^2\tau^2 \end{aligned} \tag{89}$$

$$\begin{aligned} \zeta_1^{(3)}(p,\tau) &= \frac{\pi}{2} + 0.1p_1 + 0.1p_2\tau \\ &+ 5\cdot 10^{-3}p_1^2\tau + 5\cdot 10^{-3}p_1p_2\tau^2 \end{aligned} \tag{90}$$

$$\begin{aligned} \mathsf{F}_1^{(3)}(p,\tau) &= 0.1p_2 + 5\cdot 10^{-3}p_1^2 + 0.01p_1p_2\tau \\ &- 4.17\cdot 10^{-6}p_1^4 + 5\cdot 10^{-4}p_1^3\tau + 5\cdot 10^{-3}p_2^2\tau^2 \end{aligned} \tag{91}$$

$$\begin{aligned} \zeta_1^{(4)}(p,\tau) &= \frac{\pi}{2} + 0.1p_1 + 0.1p_2\tau \\ &+ 5\cdot 10^{-3}p_1^2\tau + 5\cdot 10^{-3}p_1p_2\tau^2 \end{aligned} \tag{92}$$

The final Picard iteration leads to

$$\begin{aligned} z_1(p) = \zeta_1^{(4)}(p,r) &= \frac{\pi}{2} + 0.1p_1 + 0.1p_2 \\ &+ 5\cdot 10^{-3}p_1^2 + 5\cdot 10^{-3}p_1p_2 \end{aligned} \tag{93}$$

that is, the polynomial that represents the set of states $\mathcal{Z}_1$ at $t = r$. In this example, note that the iterations converged in two steps as $\zeta_1^{(4)}(p,\tau) = \zeta_1^{(3)}(p,\tau) = \zeta_1^{(2)}(p,\tau)$, but this is not a general case as mentioned in step 5 (see also [44]). To further obtain $z_2(p)$ at time $t = 2r$, $z_1(p)$ shall be used as initial condition for the next round of Picard iterations, starting at step 1. Notice that the expansion point $z_c$ is recalculated from $z_1(p)$ for $p = 0$, which is a standard practice when applying Taylor polynomials [31], [35]. In this example, this expansion point does not change, but it could in general.

## Appendix C
## Interval Bounds of a Polynomial Set

A computationally efficient method to estimate the boundary of a general polynomial set (5) is required. Herein, an interval over-approximation

$$[\check{y} - \hat{y}, \check{y} + \hat{y}] = \texttt{interval}(y(p)) \supseteq \mathcal{Y} \tag{94}$$

is used. The polynomial vector $y(p)$ of (3) is separated into the addition of: i) a constant vector $y(0)$, ii) a polynomial vector with even monomial terms $y_{\rm e}(p)$, and iii) a polynomial vector with odd monomial terms $y_{\rm o}(p)$, i.e., $y(p) = y(0) + y_{\rm e}(p) + y_{\rm o}(p)$.[10] The range of even monomials is the interval $[0, 1] = 0.5 + 0.5 \cdot [-1, 1]$, whereas the range of odd monomials is the interval $[-1, 1]$. Interval analysis [45] yields

$$\check{y} = y(0) + 0.5 \sum_u y_{{\rm e},u} \tag{95}$$

$$\hat{y} = 0.5 \sum_u |y_{{\rm e},u}| + \sum_v |y_{{\rm o},v}| \tag{96}$$

where the vectors $y_{{\rm e},u}$ and $y_{{\rm o},v}$ contain the coefficients of the monomials forming the polynomial vectors $y_{\rm e}(p)$ and $y_{\rm o}(p)$, respectively. The absolute value in (96) is taken element-wise.

## REFERENCES


[1] R. Park and E. Bancker, "System stability as a design problem," *AIEE Trans.*, vol. 48, no. 1, pp. 170–194, Jan. 1929.

[2] C. Concordia and M. Temoshok, "Resynchronizing of generators," *AIEE Trans.*, Oct. 1947.

[3] P. Kundur, J. Paserba, V. Ajjarapu, G. Andersson, A. Bose, C. Canizares, N. Hatziargyriou, D. Hill, A. Stankovic, C. Taylor, T. Van Cutsem, and V. Vittal, "Definition and classification of power system stability IEEE/CIGRE joint task force on stability terms and definitions," *IEEE Trans. Power Syst.*, vol. 19, no. 3, pp. 1387–1401, Aug. 2004.

[4] M. Pavella, D. Ernst, and D. Ruiz-Vega, *Transient Stability of Power Systems: A Unified Approach to Assessment and Control*. Kluwer Academic Publishers, 2000.

[5] P. M. Anderson and A. A. Fouad, *Power System Control and Stability*, 2nd ed., ser. IEEE Press Power Engineering Series. John Wiley & Sons, 2003.

[6] P. W. Sauer and M. A. Pai, *Power System Dynamics and Stability*. Champaign, Illinois: Stipes Publishing L.L.C., 2006.

[7] A. J. Wood and B. F. Wollenberg, *Power Generation, Operation, and Control*, 2nd ed. New York: John Wiley & Sons, 1996.

[8] Midcontinent Independent System Operator - MISO, *Business Practices Manual: Energy and Operating Reserve Markets*, MISO, Mar. 2016, BPM-002-r15.

[9] D. Gan, R. J. Thomas, and R. D. Zimmerman, "Stability-constrained optimal power flow," *IEEE Trans. Power Syst.*, vol. 15, no. 2, pp. 535–540, May 2000.

[10] D. Ruiz-Vega and M. Pavella, "A comprehensive approach to transient stability control: Part I–near optimal preventive control," *IEEE Trans. Power Syst.*, vol. 18, no. 18, pp. 1446–1453, Nov. 2003.

[11] A. A. Fouad and V. Vittal, "The transient energy function," *Int. J. Elect. Power and Energy Syst.*, vol. 10, no. 4, pp. 233–246, Oct. 1988.

[12] A. A. Fouad and J. Tong, "Stability constrained optimal rescheduling of generation," *IEEE Trans. Power Syst.*, vol. 8, no. 1, pp. 105–112, Feb. 1993.

[13] D. H. Kuo and A. Bose, "A generation rescheduling method to increase the dynamic security of power systems," *IEEE Trans. Power Syst.*, vol. 10, no. 1, pp. 68–76, Feb. 1995.

[14] R. Zárate-Miñano, T. Van Cutsem, F. Milano, and A. J. Conejo, "Securing transient stability using time-domain simulations within an optimal power flow," *IEEE Trans. Power Syst.*, vol. 25, no. 1, pp. 243–253, Feb. 2010.

[15] K. Sun, S. Likhate, V. Vittal, V. S. Kolluri, and S. Mandal, "An online dynamic security assessment scheme using phasor measurements and decision trees," *IEEE Trans. Power Syst.*, vol. 22, no. 4, p. 1935, Nov. 2007.

[16] R. Diao, V. Vittal, and N. Logic, "Design of a real-time security assessment tool for situational awareness enhancement in modern power systems," *IEEE Trans. Power Syst.*, vol. 25, pp. 957–965, 2010.


[10] An even monomial has all exponents even, whereas an odd monomial has at least one odd exponent.


[17] Integration of Variable Generation Task Force, "Variable generation power forecasting for operations," North American Electric Reliability Corporation, Princeton, NJ, Tech. Rep., May 2010.

[18] I. A. Hiskens and M. A. Pai, "Trajectory sensitivity analysis of hybrid systems," *IEEE Trans. Circuits Syst. I*, vol. 47, no. 2, pp. 204–220, Feb. 2000.

[19] I. A. Hiskens, "Power system modeling for inverse problems," *IEEE Trans. Circuits Syst. I*, vol. 51, no. 3, pp. 539–551, Mar. 2004.

[20] J. Hockenberry and B. Lesieutre, "Evaluation of uncertainty in dynamic simulations of power system models: The probabilistic collocation method," *IEEE Trans. Power Syst.*, vol. 19, no. 3, pp. 1483–1491, Aug. 2004.

[21] P. Prempraneerach, F. S. Hover, M. S. Triantafyllou, and G. E. Karniadakis, "Uncertainty quantification in simulations of power systems: Multi-element polynomial chaos methods," *J. Rel. Eng. and Syst. Safety*, vol. 95, no. 6, pp. 632–646, Jan. 2010.

[22] H. Choi, P. J. Seiler, and S. V. Dhople, "Propagating uncertainty in power-system DAE models with semidefinite programming," *IEEE Trans. Power Syst.*, to appear.

[23] T. L. Vu and K. Turitsyn, "Lyapunov functions family approach to transient stability assessment," *IEEE Trans. Power Syst.*, vol. 31, no. 2, pp. 1269–1277, Mar. 2016.

[24] ——, "A framework for robust assessment of power grid stability and resiliency," *IEEE Trans. Autom. Control*, vol. 62, no. 3, pp. 1165–1177, Mar. 2017.

[25] J. Muñoz, C. Cañizares, and K. Bhattacharya, "Affine arithmetic based methods for voltage and transient stability assessment of power systems with intermittent generation sources," in *Proc. 2013 IREP Symp. – Bulk Power Syst. Dynamics and Control – IX Optimization, Security and Control of the Emerging Power Grid*, Rethymnon, Crete, Greece, Aug. 2013.

[26] M. Althoff, "Formal and compositional analysis of power systems using reachable sets," *IEEE Trans. Power Syst.*, vol. 29, no. 5, pp. 2270–2280, Sep. 2014.

[27] C. Le Guernic, "Reachability analysis of hybrid systems with linear continuous dynamics," Ph.D. dissertation, Université Grenoble I – Joseph Fourier, Oct. 2009.

[28] A. Wittig, P. D. Lizia, R. Armellin, K. Makino, F. Bernelli-Zazzera, and M. Berz, "Propagation of large uncertainty sets in orbital dynamics by automatic domain splitting," *Celest. Mech. Dyn. Astr.*, vol. 122, no. 3, pp. 239–261, Jul. 2015.

[29] K. Makino and M. Berz, "Efficient control of the dependency problem based on Taylor model methods," *Reliable Computing*, vol. 5, no. 1, pp. 3–12, Feb. 1999.

[30] ——, "Suppression of the wrapping effect by Taylor model-based verified integrators: Long-term stabilization by shrink wrapping," *Int. J. Diff. Equations and Applicat.*, vol. 10, no. 4, pp. 385–403, 2005.

[31] K. Makino, "Rigorous analysis of nonlinear motion in particle accelerators," Ph.D. dissertation, Michigan State University, 1998.

[32] K. Makino and M. Berz, "Verified integration of ODEs and flows using differential algebraic methods on high-order Taylor models," *Reliable Computing*, vol. 4, pp. 361–369, 1998.

[33] S. Wang, Z. Zheng, and C. Wang, "Power system transient stability simulation under uncertainty based on Taylor model arithmetic," *Proc. Frontiers Elect. and Electron. Eng. in China*, vol. 4, no. 2, pp. 220–226, Jun. 2009.

[34] M. Berz, *Modern Map Methods in Particle Beam Physics*. London, UK: Academic Press, 1999.

[35] M. Berz and G. Hoffstätter, "Computation and application of Taylor polynomials with interval remainder bounds," *Reliable Computing*, vol. 4, pp. 83–97, 1998.

[36] E. A. Coddington and N. Levinson, *Theory of Ordinary Differential Equations*. McGraw-Hill, 1955.

[37] K. Makino and M. Berz, "Rigorous integration of flows and ODEs using Taylor models," in *Proc. 2009 Conf. Symbolic Numeric Computation*, Kyoto, Japan, Aug. 2009.

[38] J. K. Scott, B. Chachuat, and P. I. Barton, "Nonlinear convex and concave relaxations for the solutions of parametric ODEs," *Optimal Control Application and Methods*, vol. 34, no. 2, pp. 145–163, Mar./Apr. 2013.

[39] Energy Development and Power Generation Committee, *IEEE Recommended Practice for Excitation System Models for Power System Stability Studies*, IEEE Power Engineering Society Std. 421.5-2005, Apr. 2006.

[40] IEEE committee report, "Computer representation of excitation systems," *IEEE Trans. Power App. Syst.*, vol. PAS-87, no. 6, pp. 1460–1464, Jun. 1968.
[41] Wind Generation Task Force, "The technical basis for the new WECC voltage ride-through (VRT) standard," Western Electricity Coordinating Council (WECC), Tech. Rep., Jun. 2007.
[42] P. C. Krause, O. Wasynczuk, S. D. Sudhoff, and S. Pekarek, *Analysis of Electric Machinery and Drive Systems*, 3rd ed. New York: IEEE Press, Wiley-Interscience, 2013.
[43] (2015) MATLAB R2015a. The MathWorks Inc. Natick, MA. [Online]. Available: http://www.mathworks.com
[44] X. Chen, S. Sankaranarayanan, and E. Ábrahám, "Taylor model flowpipe construction for nonlinear hybrid systems," in *Proc. 33rd IEEE Real-Time Syst. Symp.*, San Juan, PR, Dec. 2012.
[45] R. E. Moore, R. B. Kearfott, and M. J. Cloud, *Introduction to Interval Analysis*. Philadelphia, PA: SIAM, 2009.